Cano-Pleite, E.; Hernández-Jiménez, F.; Acosta-Iborra, A. (2015) Compressible-gas two-fluid modeling of isolated bubbles in a vertically vibrated fluidized bed and comparison with experiments. *Chemical Engineering Journal*, v. 271, pp.: 287-299.

DOI: https://doi.org/10.1016/j.cej.2015.02.096

Compressible-gas two-fluid modeling of isolated bubbles in a vertically vibrated fluidized bed and comparison with experiments.

E. Cano-Pleite[a,*], F. Hernández-Jiménez[a], A. Acosta-Iborra[a]

[a] *Carlos III University of Madrid, Department of Thermal and Fluid Engineering, Av. de la Universidad 30, 28911 Leganés, Madrid, Spain*

Abstract

In this work the size and motion of isolated bubbles in a vertically vibrated fluidized bed are numerically investigated by means of two-fluid model simulations. The oscillations of the bed bulk and the bubble diameter and velocity are compared with experimental results of a pseudo-2D bed using an averaging of cycles method to account for the intrinsic unsteadiness caused by vibration. The effects of gas compressibility and the air plenum of the vibrated bed are also numerically investigated. The results show that the two-fluid model simulations resorting to a compressible gas model are able to reproduce both the cyclic compression and expansion of the bed bulk and the bubble oscillations observed in the experiments. In contrast, the simulations with the incompressible gas model fail to reproduce these effects. The presence of the air plenum in the numerical model diminishes the amplitude of the bed and bubble oscillations and improves their resemblance to the experiments. In the simulations with compressible gas, a phase delay is found between the bed displacement and the oscillation of bubble characteristics. In harmony with experiments, the phase delay is smaller in the lower half of the bed (i.e. close to the distributor) than in the upper half. This effect is not reproduced by the simulations with incompressible gas-phase. These results suggest that the phase delay in vibrated beds is caused by the compression of the gas phase, which leads to compression-expansion waves traveling through the bed. The simulations also confirm that the amplitude of vibration influences the magnitude of the bubble diameter and velocity oscillations, whereas the delay of the bubble characteristics is mainly affected by the bed vibration frequency.

Keywords: Fluidization, Two-fluid model, Bubble, Vibrated fluidized bed, Oscillation, Compressibility

1. Introduction

Fluidization is a process widely used in chemical reactors and materials processing due to the good efficiency it provides in solid-solid and gas-solid contacts [1]. Nevertheless, agglomeration or channeling of fine particles may occur, which can end up defluidizing the bed. Several strategies have been employed to

*Corresponding author. Tel:+34 91 624 8884
Email address: edcanop@ing.uc3m.es (E. Cano-Pleite)

improve fluidization homogeneity, e.g. the introduction of a mechanical stirrer or the pulsation of the gas flow [2]. Many efforts have been made to modify the particle and bubble behavior in a fluidized bed also by external means. For example, ferromagnetic particles subjected to magnetic fields can change the way the bed fluidizes, extending the bubble-free operation range in fluidization state [3] or diminishing the bubble size [4]. Acoustic fields have also been employed for the improvement of the fluidization quality of group C cohesive powders [5].

Mechanical vibration of fluidized beds, i.e. vibrating fluidized beds (VFB), is a fluidization technology consisting in introducing vibratory kinetic energy to a conventional fluidized bed [6–9]. Vibration of the bed reduces minimum fluidization velocity [10], and provides the necessary energy to break interparticle bonds, reduce agglomerates and avoid channeling. Thus, it is a very effective technique for the fluidization of cohesive particles [11, 12], drying of granular material [13, 14], agglomeration control [15] and control of particle segregation [16].

Existing experimental and simulation studies of bubbles in VFBs are mainly centered on beds working under bubbling regime [9, 17–23]. Global indicators such as bubble mean diameter and velocity [9, 17–19, 24], air pressure and void fraction fluctuations [21, 22] as well as solids circulation promoted by vibration [23] are included in these works, in which the presence of multiple interacting bubbles complicates the elucidation of the basic effects that vibration induces on each individual bubble. Eccles and Mujumdar [24] studied a train of bubbles in a vibrated thin bed. Zhou et al. [9] carried out experiments to study the particle flow pattern and its interaction with bubble paths, pressure drop and bed expansion ratio in a pseudo two-dimensional (2D) bed filled with spherical particles of 198 μm and subjected to horizontal and vertical vibration. Also, Mawatari et al. [17] and Zhou et al. [18] experimentally studied pseudo-2D beds under vertical vibration, using particles of 60 μm and 198 μm of average diameter, respectively. The vibrated bed conditions of [18] were reproduced by Acosta-Iborra et al. [19] using two-fluid models simulations. All these three studies [17–19] revealed that, once a fluidized bed is vibrated, the averaged bubble diameter increased with the amplitude or frequency of vibration, though a more complicated dependence was experienced by the averaged bubble velocity. In an attempt to better understand the intricate behavior of bubbles in vibrating fluidized beds, Cano-Pleite et al. [25] experimentally studied isolated bubbles in a pseudo-2D fluidized bed subjected to vertical vibration. Using digital image analysis (DIA) techniques, they captured the individual oscillation of the size and velocity of solitary bubbles and the oscillation of the bulk of the bed.

Numerical simulation of fluidized beds can be employed as a tool to improve the understanding the complex behavior of fluidized beds during vibration. Besides, once a simulation model is experimentally validated, it can also be used for the design and scale-up of vibrating fluidized beds due to the unrestricted availability of data, the lack of interferences and the null measurement errors present in the simulation. Two main kinds of models have been reported in the literature for the simulation of vibrated fluidized beds: the Lagrangian-Eulerian and the Eulerian-Eulerian models. Nearly all the reported simulations of VFBs resort

to the Lagrangian-Eulerian model based on the discrete element modeling (DEM) of the bed particles. In this model the motion of each particle is individually simulated and coupled with the Eulerian CFD simulation of the gas field (CFD-DEM) if the bed is aerated. For the coupling, semi empirical air-to-particle drag models are used. Despite its promising results, the Lagrangian-Eulerian method is still restricted to a relatively small number of particles (i.e. order of 10^6) that makes challenging the escalation of results to medium or large size VFBs plants.

Tatemoto et al. [21] and Xiang et al. [22] employed the Lagrangian-Eulerian (CFD-DEM) method to simulate the motion of particles in a reduced two-dimensional VFB in which the bed thickness of the simulated bed was equal to the particle diameter and 1500 particles were considered. Particle velocity and concentration of particles were studied, giving a qualitative understanding of VFB behavior and the vibration energy transmission [22]. A study on gas velocity and the change of void fraction and pressure fluctuations as a function of the time under different vibration modules was carried out in the work by Tatemoto et al. [21]. However, as stated in [22], a quantitative understanding of this kind of results is difficult given the low number of particles employed in the simulations. Three-dimensional (3D) simulations were performed by Limtrakul et al. [26] in a cylindrical vibrated fluidized bed of 2.41 mm of diameter filled with cohesive particles. The effects of particle type, superficial gas velocity and vibration amplitude and frequency on particle movement and velocity vectors were analyzed. More recently, Zeilstra et al. [23] used combined PIV measurements and CFD-DEM simulations to study solid circulation rates in a pseudo-2D vibrated fluidized bed. Although the results obtained were in good qualitative agreement with the experiments and the literature, the bed size was still small (15 x 1.5 x 60 cm^3) and the particle size was relatively large (1 mm diameter) because of restrictions caused by the high computational cost of the CFD-DEM simulations.

As an answer to the difficulties of the Lagrangian-Eulerian (CFD-DEM) simulations, Acosta-Iborra et al. [19] proposed the simulation of vibrated fluidized beds by solving the two-fluid (Eulerian-Eulerian) model CFD equations [27, 28] in a coordinate system that moves with the bed. Thus, vibration is transformed into acceleration terms that are introduced in the simulations as body forces in both the gas and particle phases. Using this methodology, the size of the bed and number of particles represented that can be simulated can be increased dramatically compared to the Lagrangian-Eulerian alternatives, making affordable the numerical simulation of bigger VFBs facilities. Since particles are treated as a continuum interpenetrated by the gas phase in two-fluid model simulations, additional closure models to those used in DEM simulations are required in two-fluid models to reproduce the particle-particle and particle-wall interactions [28].

Although some of the previous numerical works of VFBs consider the gas phase as a compressible medium [22, 23, 26], it is not totally clear whether the compressibility of the gas phase plays an important role on the VFB behavior and in particular on the oscillatory motion of bubbles. However, to the author's best knowledge, existing numerical studies regarding vibrating fluidized beds do not investigate the influence of the gas phase compressibility on the fluctuations induced by vibration in the bed.

The present work is aimed at numerically studying the behavior of isolated bubbles in a vertically vibrated fluidized bed using a two-fluid model that includes the compressibility of the gas phase. Aside from testing the capabilities of two-fluid models in reproducing the experimental results of oscillatory size and displacement of bubbles in a pseudo-2D bed reported by Cano-Pleite et al. [25], the present simulation study is also intended to elucidate the effect of the gas compressibility on the bulk of the bed and the bubble motion. Similarly to the experiments in Cano-Pleite et al. [25], the simulation results are presented using an averaging of cycles method. Using this method, the local fluctuations caused by the bed vessel vibration on the bed bulk and the bubble velocity and diameter can be systematically analyzed and compared to the experimental observations. Besides, the effect of vibration amplitude and frequency on the oscillation of isolated bubbles in the simulated bed is studied and compared to that of the experiments. The results show that the two-fluid model simulation with compressible gas phase is capable of well reproducing the experimental behavior of isolated bubbles in a vibrated fluidized bed, whereas this is not true if the gas is simulated as an incompressible phase. This important outcome suggests that the gas-phase compressibility is one of the main mechanisms of information propagation inside the bed.

2. Vibrated fluidized bed system

The system simulated in this work is a two-dimensional bed of dimensions 0.3 x 0.6 m^2 (width W and height H), that is a 2D replica of the experimental facility employed by Cano-Pleite et al. [25], which consists of a pseudo-2D fluidized bed of dimensions 0.3 x 0.6 x 0.01 m^3 (width, height and thickness, respectively) placed on a vibrating structure. The air distributor consists of a perforated plate with one row of 20 holes of 1 mm diameter that are spaced 1.5 cm apart covering all the distributor section. In [25] the bed was filled with ballotini glass beads with a mean diameter of 213 μm and a density of 2500 kg/m^3 (type B particles according to Geldart's classification) with a minimum fluidization velocity of $U_{mf} = 0.055$ m/s. The settled bed height was set to $h_0 = 0.45$ m for all the experiments conducted.

Two independent air supplies at ambient temperature (298 K) were employed in the experiments [25]. A principal air supply was used for setting the bed under minimum fluidization conditions. Bubbles were sequentially injected through a secondary air supply, which is an orifice drilled on the centre of the back wall of the bed and situated 5 cm above the distributor. The average rate of bubble injections was 25-30 bubbles per minute.

The bulk of the bed was recorded in the experimental facility using a using a digital camera, BASLER A640, which took images the front view of the fluidized bed at a rate of 100 images per second. These images were used to characterize the bubble size and motion as well as the bed bulk and the bed vessel vibration amplitude and frequency. More details about the experimental set-up can be found in [25].

Table 1: Governing equations

ine Continuity equations

$$\frac{\partial}{\partial t}(\varepsilon_p \rho_p) + \nabla \cdot (\varepsilon_p \rho_p \boldsymbol{U}_p) = 0 \qquad \text{(T1.1)}$$

$$\frac{\partial}{\partial t}(\varepsilon_g \rho_g) + \nabla \cdot (\varepsilon_g \rho_g \boldsymbol{U}_g) = 0 \qquad \text{(T1.2)}$$

Momentum equations

$$\left[\frac{\partial}{\partial t}(\varepsilon_p \rho_p \boldsymbol{U}_p) + \nabla \cdot (\varepsilon_p \rho_p \boldsymbol{U}_p \boldsymbol{U}_p)\right] = -\varepsilon_p \nabla P_g + \nabla \cdot \boldsymbol{\tau}_p + \boldsymbol{I}_{gp} + \varepsilon_p \rho_p \boldsymbol{f}_{p,eq} \qquad \text{(T1.3)}$$

$$\left[\frac{\partial}{\partial t}(\varepsilon_g \rho_g \boldsymbol{U}_g) + \nabla \cdot (\varepsilon_g \rho_g \boldsymbol{U}_g \boldsymbol{U}_g)\right] = -\varepsilon_g \nabla P_g + \nabla \cdot \boldsymbol{\tau}_g - \boldsymbol{I}_{gp} + \varepsilon_g \rho_g \boldsymbol{f}_{g,eq} \qquad \text{(T1.4)}$$

Granular temperature equation

$$\frac{3}{2}\rho_p \left[\frac{\partial \varepsilon_p \Theta}{\partial t} + \nabla \cdot (\varepsilon_p \boldsymbol{U}_p \Theta)\right] = \nabla \cdot (\kappa_\Theta \nabla \Theta) + (-P_s \bar{\bar{I}} + \boldsymbol{\tau}_s) : \nabla \boldsymbol{U}_s + \Pi_p - \varepsilon_p \rho_p J_p \qquad \text{(T1.5)}$$

ine

3. Two-Fluid modelling of vibrating fluidized bed

The experimental conditions previously described were numerically reproduced in this work using a two-fluid model (TFM) strategy. As commented in the introduction section, the TFM allows for an Eulerian-Eulerian description of the fluidized bed, the gas phase (g) and the particles or solids phase (p) being modeled as two interpenetrating continua. Here, the MFIX code (Multiphase Flow with Interphase eXchanges) [29, 30] was used to solve the conservation equations of mass and momentum for each of the phases (see Equations T1.1-4 in Table 1) and the equation of transport of granular temperature Θ, which accounts for the level of random fluctuation of particle velocity due to collisions (Equation T1.5 in Table 1). The kinetic theory of granular flow (KTGF) [27] was used for the closure of the solids pressure and stress terms. For the calculation of the drag coefficient between the gas and the particles K_{gp} the drag model by Gidaspow [27] was selected in this work because of its robustness during the start-up of the simulation. Other closure models employed in the present study are summarized in Table 2 [29].

Following the methodology proposed by Acosta-Iborra et al. [19], the procedure conducted here to introduce the oscillatory displacement of the bed vessel in the simulation consists in the solution of the governing equations using a system of reference that moves with the base of the bed vessel. After performing this change in the governing equations, vibration appears in the two-fluid model constitutive equations as an equivalent mass force (see Table 1) acting in both the gas and the solid momentum balance equations:

Table 2: Closure models

ine Drag coefficient between gas and particles

$$K_{gp} = \begin{cases} \frac{3}{4} C_D \frac{\rho_g \varepsilon_g \varepsilon_p |\boldsymbol{U}_g - \boldsymbol{U}_p|}{d_p} \varepsilon_g^{-2.65} & \varepsilon_g \geq 0.8 \\ 150 \frac{\varepsilon_p^2 \mu_g}{\alpha_g d_p^2} + 1.75 \frac{\varepsilon_p \rho_g |\boldsymbol{U}_g - \boldsymbol{U}_p|}{d_p} & \varepsilon_g < 0.8 \end{cases} \quad \text{(T2.1)}$$

$$C_D = \begin{cases} \frac{24}{Re}(1 + 0.15 Re^{0.687}) & Re < 1000 \\ 0.44 & Re \geq 1000 \end{cases} \quad \text{(T2.2)}$$

$$Re = \frac{\rho_g \varepsilon_g |\boldsymbol{U}_g - \boldsymbol{U}_p| d_p}{\mu_g} \quad \text{(T2.3)}$$

Gas/solids momentum interface exchange

$$\boldsymbol{I}_{gp} = K_{gp}(\boldsymbol{U}_g - \boldsymbol{U}_p) \quad \text{(T2.4)}$$

Gas stress tensor

$$\boldsymbol{\tau}_g = 2\mu_{ge} \boldsymbol{S}_g \quad \text{(T2.5)}$$

$$\boldsymbol{S}_g = \frac{1}{2}\left(\nabla \boldsymbol{U}_g + (\nabla \boldsymbol{U}_g)^T\right) - \frac{1}{3} \nabla \cdot \boldsymbol{U}_g \boldsymbol{I} \quad \text{(T2.6)}$$

Solid stress tensor

$$\boldsymbol{\tau}_p = (-P_p + \eta \mu_b \nabla \cdot \boldsymbol{U}_p)\, \bar{\bar{I}} + 2\mu_p \bar{\bar{S}}_p \quad \text{(T2.7)}$$

$$\boldsymbol{S}_p = \frac{1}{2}\left(\nabla \boldsymbol{U}_p + (\nabla \boldsymbol{U}_p)^T\right) - \frac{1}{3} \nabla \cdot \boldsymbol{U}_p \boldsymbol{I} \quad \text{(T2.8)}$$

Solids pressure

$$P_p = \varepsilon_p \rho_p \Theta \left[1 + 4\eta \varepsilon_p g_0\right] \quad \text{(T2.9)}$$

$$g_0 = \frac{1 - 0.5\varepsilon_p}{(1 - \varepsilon_p)^3} \quad \text{(T2.10)}$$

ine

Solids viscosity

$$\mu_p = \left(\frac{2+\alpha}{3}\right)\left[\frac{\mu_p^*}{g_0 \eta (2-\eta)}\left(1 + \frac{8}{5}\eta \varepsilon_p g_0\right)\cdot \left(1 + \frac{8}{5}\eta(3\eta - 2)\varepsilon_p g_0\right) + \frac{3}{5}\eta \mu_b\right] \quad \text{(T2.11)}$$

$$\mu_p^* = \frac{\rho_p \varepsilon_p g_0 \Theta \mu}{\rho_p \varepsilon_p g_0 \Theta + \left(\frac{2 K_{gp} \mu}{\rho_p \varepsilon_p}\right)} \quad \text{(T2.12)}$$

$$\mu = \frac{5}{96} \rho_p d_p \sqrt{\pi \Theta} \quad \text{(T2.13)}$$

$$\mu_b = \frac{256}{5\pi} \mu \varepsilon_p^2 g_0 \quad \text{(T2.14)}$$

Collisional dissipation

$$J_p = \frac{48}{\sqrt{\pi}} \eta (1 - \eta) \frac{\varepsilon_p g_0}{d_p} \Theta^{3/2} \quad \text{(T2.15)}$$

$$\eta = \frac{1 + e}{2} \quad \text{(T2.16)}$$

Exchange terms

$$\Pi_p = -3 K_{gp} \Theta + \frac{81 \varepsilon_p \mu_g^2 |\boldsymbol{U}_g - \boldsymbol{U}_p|^2}{g_0 d_p^3 \rho_p \sqrt{\pi \Theta}} \quad \text{(T2.17)}$$

Schaeffer's [31] frictional stress model

$$P_{p,fric} = \begin{cases} 10^{24}(\varepsilon^* - \varepsilon_g)^{10} & \varepsilon_g < \varepsilon^* \\ 0 & \varepsilon_g \geq \varepsilon^* \end{cases} \quad \text{(T2.18)}$$

$$\mu_f = \begin{cases} min\left(\frac{P_{p,fric} \sin(\theta)}{\sqrt{4 I_{2Dp}}}, \mu_s^{max}\right) & \varepsilon_g < \varepsilon^* \\ 0 & \varepsilon_g \geq \varepsilon^* \end{cases} \quad \text{(T2.19)}$$

$$\mu_s^{max} = 100 \text{ Pa·s} \quad \text{(T2.20)}$$

$$\boldsymbol{f}_{m,eq} = \boldsymbol{g} - \boldsymbol{a}(t) \tag{1}$$

where $\boldsymbol{g}$ is the gravity acceleration vector and $\boldsymbol{a}(t)$ accounts for the acceleration of the bed vessel induced by vibration. Considering a vertical sinusoidal displacement of the bed vessel, $\delta(t) = A\sin(\omega t)$, the bed vessel acceleration term can be expressed as follows:

$$\boldsymbol{a}(t) = -A\omega^2 \sin(\omega t)\boldsymbol{u}_z \tag{2}$$

where A represents the vibration amplitude, $\omega = 2\pi f$ is the angular frequency of vibration, f is the vessel vibration frequency and $\boldsymbol{u}_z$ is the vertical unitary vector. More information concerning this transformation of equations can be found in Acosta-Iborra et al. [19].

3.1. Treatment of gas compressibility

The presence of an oscillatory vibration displacement of the bed vessel promotes the generation of compression-expansion waves which travel through the bed [25, 32, 33]. These waves may affect the gas density of the bed. Thus, the compressibility of the gas phase was considered in the numerical models employed in this work using the ideal gas law to calculate the gas density at each point and time instant during the two-fluid model simulation:

$$\rho_g = \frac{P_g}{R_g T_g} \tag{3}$$

where P_g is the gas pressure, $T_g = 298$ K is the gas temperature, and $R_g = 287$ J/Kg K is the ideal gas constant for air. It is assumed that the process in all the bed is isotherm since real particles accumulate heat and damp small fluctuations of temperature [34]. The compressible gas TFM simulations were compared to those in which the gas phase was considered incompressible ($\rho_g = 1.22$ kg/m^3).

3.2. Numerical solution and boundary conditions

In order to reproduce the VFB system described in Section 2, two simulation domains are proposed in this work. The two domains are two-dimensional reproductions of the fluidized bed employed in [25]. In the first domain, the air flow velocity through the distributor is directly imposed, as usually done, excluding the simulation of the plenum. The second domain, to fully account for the effect of the plenum in the simulation, adds to the previous domain a plenum of equivalent height H_{eq} [35], $H_{eq} = V_{ap}/A_{ap}$, where V_{ap} and A_{ap} are, respectively, the plenum chamber volume and the cross-sectional area of the experimental bed. In this second computational domain, the air distributor was numerically modeled as an internal semipermeable surface, which prevents the particles from falling to the plenum and allows for the gas to cross the distributor with a pressure drop made equal to that of the actual distributor. Both kinds of computational domains

are discretized with a square grid of cell size equal to 4 mm in the section occupied by the solids. The cells are slightly elongated in the sections on top of the bed and in the plenum, where only gas is present (see Figure 1). This leds to a total number of cells of 11704 for the case without plenum and 19943 for the case with plenum. Sensitivity results in previous works [19] showed a good reproduction of bubble characteristics for a mesh of greater cell size. Given the large number of cases considered, and the need of computing the transient solution for a physical time period sufficiently large to obtain statistically meaningful results, no attempt was made to simulate the pseudo-2D bed in three dimensions in this work.

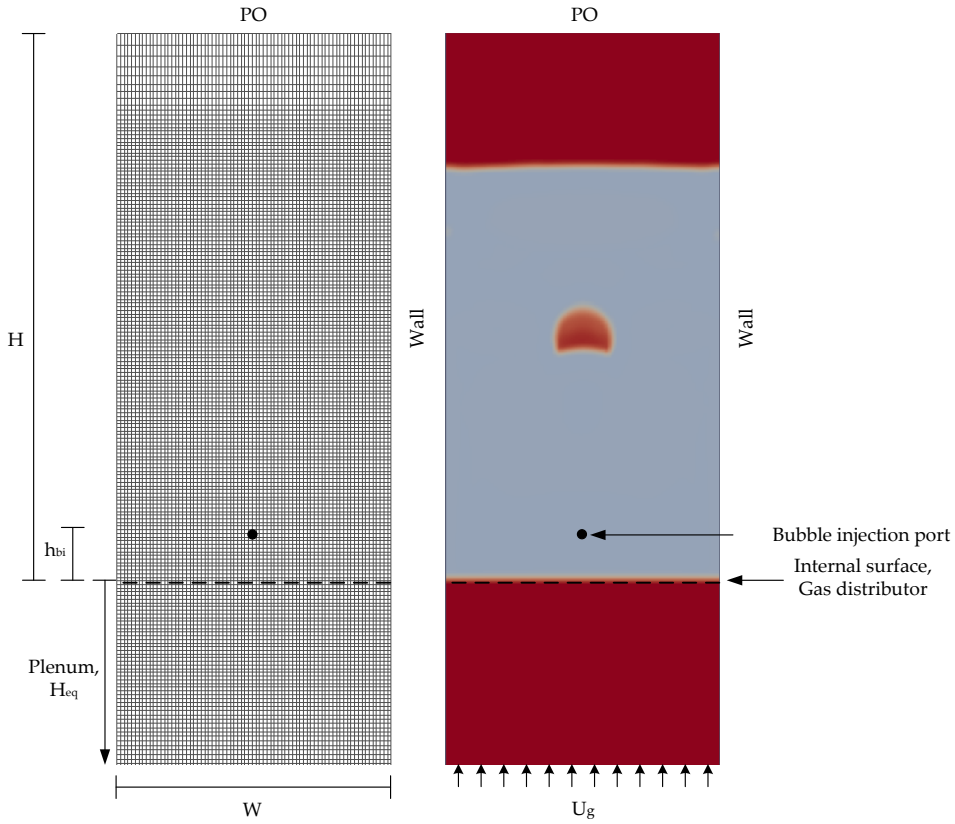

Figure 1: Computational domain (case with plenum) and boundary conditions of the simulations.

To study bubble oscillating characteristics, the simulation results were exported each $5 \cdot 10^{-3}$ s over a period of 120 s of physical time in each of the cases conducted. The air was uniformly introduced through the distributor (case without plenum) and through the bottom of the plenum (case with plenum) at a given velocity U_g, to set the bed under minimum fluidization conditions. In order to reproduce the experimental conditions of Cano-Pleite et al. [25], bubbles were injected in the bed through a punctual source of air of 4 mm x 4 mm situated 5 cm above the distributor. The amount of mass injected in each of the bubbles in the subsequent simulations was set to statistically match the size of the bubbles found in the experiments.

Table 3: Simulation conditions

ine Parameter	Value	Parameter	Value
ine W(mm)	300	H(mm)	600
$d_p(\mu$m)	213	ρ_p(kg/m^3)	2500
U_g (m/s)	0.04	μ_g(Pa s)	$1.86 \cdot 10^{-5}$
h_0(m)	0.45	H_{eq}(m)	0.84
h_{bi}(m)	0.05	e(-)	0.9
ε_0(-)	0.4	ε^*(-)	0.4
$\theta(^o)$	30	Δt_{exp}(s)	0.005
ine			

The mean and the standard deviation of the bubble diameter were obtained from the experiments and these values were introduced in the simulations by means of Equation (4), which incorporates a random function that accounts for the different volume injected in each bubble of the experiments. In particular, for each bubble, air was injected until the equivalent-area diameter of the bubble D_{inj} reached:

$$D_{inj} = D_{be} + 2\sqrt{3}\sigma_{be}(\text{Rand} - 0.5) \tag{4}$$

where D_{be} and σ_{be} are, respectively, the experimental mean bubble diameter and the bubble diameter standard deviation. Rand stands for a randomly generated number between 0 and 1. Equation (4) gives a diameter distribution of mean value and standard deviation similar to the experiments.

At the exit, a pressure outlet boundary condition was specified, with a static pressure equal to one atmosphere. At the walls of the bed and the plenum, no-slip conditions were imposed for the gas phase. For the solids, partial-slip conditions of Johnson and Jackson [36] were specified at the walls with a standard specularity coefficient of $\Phi = 0.6$. A restitution coefficient of 0.9 was used for both the particle-particle and particle-wall collisions. Similarly to the experiments in [25], the static bed height in all the cases was set to $h_0 = 0.45$ m. These simulation conditions are summarized in Table 3.

The simulation cases carried out are listed in Table 4. The base conditions of vibration frequency and amplitude are $f = 13.9$ Hz and $A = 2.7$ mm. To account for the effects of not introducing gas compressibility, an initial case with constant ρ_g was considered (Case-1). In this incompressible gas case, there was no need of introducing the plenum of the bed since compression waves cannot occur. Investigations on the effect of not including the plenum when the gas is compressible are performed by means of Case-2. Finally, the effect of vibration amplitude and frequency is studied with the rest of cases of Table 4. In Cases 3, 4 and 5 the vibration amplitude is varied whereas Cases 3, 6 and 7 comprise different vibration frequencies.

Table 4: List of simulated cases

ine Case	Gas phase	Plenum	f (Hz)	A (mm)
ine 1	Incompressible	No	13.9	2.7
2	Compressible	No	13.9	2.7
3	Compressible	Yes	13.9	2.7
4	Compressible	Yes	13.9	4.1
5	Compressible	Yes	13.9	5.7
6	Compressible	Yes	10.8	3
7	Compressible	Yes	17.2	2.5
ine				

4. Data processing

4.1. Bubble detection

The bubbles in the simulation were identified by setting a common threshold value of $\varepsilon_{p,th} = 0.2$ [37, 38] on the instantaneous solids volume fraction. Visual inspection of results showed that this threshold ensured the robustness of the location of the bubble contour in the VFB simulations. Greater values of $\varepsilon_{p,th}$ led to a growth of the bubble contour oscillation with a lost of resolution in defining the bubble contour. Thus, for each simulation frame of solid volume fraction, a point in the image was assigned a value of 0 if $\varepsilon_p < \varepsilon_{p,th}$ or 1 if $\varepsilon_p > \varepsilon_{p,th}$, making the contour of the bubble easily identifiable. Following previous works [19, 39, 40], the bubble equivalent diameter was calculated as the diameter of a circle having the same area of the bubble.

The bubble vertical position (z_b) was calculated as the distance of the bubble centroid to the distributor. The bubble vertical velocity was computed as the vertical displacement of the bubble centroid between two consecutive simulation frames (i.e. $\Delta t_{exp} = 0.005$ s). In particular, the bubble velocity was calculated in an absolute system of reference not attached to the distributor so that:

$$V_b = \frac{z_b(t + \Delta t_{exp}) + \delta(t + \Delta t_{exp}) - z_b(t) - \delta(t)}{\Delta t_{exp}} \tag{5}$$

Note that changes of shape of a bubble may produce an apparent displacement that is difficult to separate from the main bubble motion. In the results, the bed volume is calculated as the frontal area of the bed, including bubbles, times the bed thickness.

4.2. Averaging of cycles

In order to study the oscillatory behavior of both the bed bulk and the bubble characteristics, an averaging of cycles method was employed, as in [25]. For a given variable $y(t)$, the oscillation Δy is calculated by subtracting the moving average, $\overline{y}(t)$ of $y(t)$, performed within a time interval $[-T/2, T/2]$, from the instantaneous value, i.e. $\Delta y(t) = y(t) - \bar{y}(t)$. It is considered that the main oscillatory behavior of $y(t)$ is caused by vibration. Thus, for a periodic oscillation of the bed vessel of angular frequency $\omega = 2\pi f$, each

instantaneous value of $\Delta y(t)$ is associated to a phase ϕ, where $\phi = 0$ corresponds to the beginning of a cycle (bed vessel at its central position $\delta = 0$ and moving upwards) and $\phi = 2\pi$ to the end of the cycle (bed vessel at its central position $\delta = 0$ and moving again upwards). The averaging of cycles method promediates the cyclic values of $\Delta y(t)$ in a finite number of phase intervals, $N_\phi = 20$, as follows:

$$\overline{\Delta y}(\phi) = \frac{1}{N_{tot}} \sum_{n=1}^{N_{tot}} \Delta y \left(\frac{\phi + 2\pi n}{\omega} \right) \tag{6}$$

where N_{tot} is the number of periodic cycles of the bed vessel vibration. More details about the averaging of cycles method employed in the present work can be found in [25].

To analyze the variation of the bubble behavior with the distance to the distributor, the averaging of cycles performed in Equation (6) was done for bubbles whose centroid was situated in the lower height interval of the bed $z = 0.1 - 0.275$ m (lower half volume of the bed) and in the upper height interval $z = 0.275 - 0.45$ m (upper half volume of the bed).

A 5th order polynomial fitting to the averaged oscillation results was included just for enhancing the visual inspection of the results, and no attempt was made to perfectly reproduce the periodicity of the oscillations.

4.3. Phase delay of oscillations

The retardation in phase ϕ of the oscillation of a variable with respect to a reference signal (i.e. the bed vessel displacement or velocity) is the phase delay ϕ_d. This phase delay is estimated using Equation (7), in which ϕ_d is the value of x that minimizes the squared difference between the phase averaged fluctuation signal ($\overline{\Delta y}_i$) and a reference sinusoidal signal whose amplitude $A_{\overline{\Delta y}}$ is made equivalent to the amplitude of $\overline{\Delta y}_i$:

$$\min_x \left(\sum_{i=1}^{N_\phi} [\overline{\Delta y}_i - A_{\overline{\Delta y}} \sin(\phi_i - x)]^2 \right) \longrightarrow \phi_d = x \tag{7}$$

$$A_{\overline{\Delta y}} = \sigma_{\overline{\Delta y}} \sqrt{2} \tag{8}$$

where $\sigma_{\overline{\Delta y}}$ is the standard deviation of $\overline{\Delta y}$. Positive values of x in Equation (7) correspond to a positive phase delay, i.e. $\overline{\Delta y}$ is retarded in time with respect to the bed vessel displacement. The reference signal is a cosine instead of a sine in Equation (7) when the reference signal is the bed vessel velocity instead of the displacement. Sensitive analysis of the results showed that the number of intervals N_ϕ, employed to represent the oscillations of a given variable, has little influence on ϕ_d.

5. Results and discussion

The results presented in this work are structured as follows. Firstly, the bed general motion, the effect of gas compressibility and the presence of the plenum in the bed are studied by comparison of the simulation results with experimental evidence (Section 5.1). Secondly, the same methodology is followed for the study of the effect of vibration on bubble diameter (Section 5.2) and velocity fluctuations (Section 5.3) caused by vibration and their variation with the bed vessel vibration amplitude and frequency.

5.1. General dense phase and bubble behavior

The vertical vibration of the bed vessel promotes a displacement of the bed bulk, which has been experimentally demonstrated to have an impact on the bed and bubble dynamics [25]. Figure 2a shows the time evolution of the volume of the simulated VFB, normalized with the settled bed volume h_0WK, when an isolated bubble is rising in the bed. It can be observed that, for the three cases, the bed volume oscillates with a frequency similar to the vibration frequency of the bed vessel, ω. However, the volume of the bed simulated with the incompressible gas-phase model oscillates with a markedly smaller amplitude than the simulated bed with the compressible gas. According to Figure 2, the simulation of the bed with the plenum together with the compressible gas model (Case-3) seems to partially relax the bed fluctuations, which lead to less vigorous oscillation of the bed volume compared with the same simulations with compressible gas but without plenum. Also, the phase of the bed volume oscillations in the incompressible case is ahead of the phase of the results calculated with the compressible gas model. Figure 2b contains the location of the centroid of the simulated bubble the period of time shown in Figure 2a. While the bubble is rising, the bubble centroid vertical position increases and this movement slightly fluctuates since it is simultaneously affected by the oscillation of the bed volume.

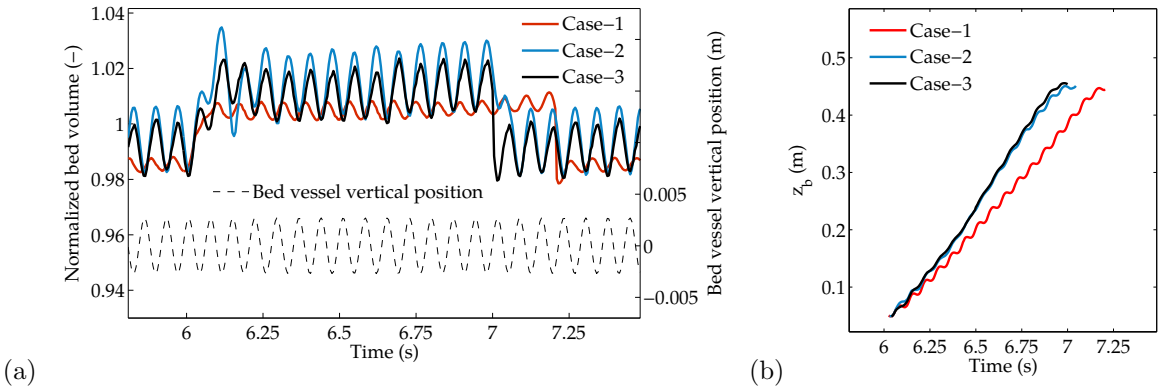

Figure 2: (a) Normalized bed volume and (b) bubble absolute vertical position as a function of the time for the incompressible gas-phase model (Case-1), compressible gas-phase model without plenum (Case-2) and compressible gas-phase model with plenum (Case-3). $f = 13.9$ Hz and $A = 2.7$ mm.

The amplitude and phase of the bed volume oscillations can be more easily analyzed by means of the averaging of cycles method described in Section 4.2. The simulation and experimental results are shown in Figure 3. The averaged oscillations of the simulated bed volume with compressible gas present an opposition in phase with respect to the bed displacement, i.e. when the bed vessel is moving upwards, the bed surface is moving downwards and vice-versa. Thus, the bed volume reaches its minimum when the bed vessel is at its higher position, i.e. the bed is compressed, and it is maximum when the vessel is at its lower point, i.e. the bed is expanded. This behavior of the simulated bed is in very good agreement with the experiments, as shown in Figure 3. It is clear from the figure that the simulation of the bed with incompressible gas leads to inaccurate results since the phase and the amplitude of the bed volume is different to the experimental results. Thus, the results presented in Figure 3 can be understood as a cyclic compression-expansion of the bed caused by the compression of the gas phase in the bed bulk. Besides, the magnitude of the cyclic compression-expansion of the bed is overestimated when the plenum chamber is not considered in the simulation. The fact that the presence of the plenum does not promote a change on the phase of the bed volume oscillation but decreases the amplitude of the bed volume oscillation corroborates that the expansion-compression of the bed volume is commanded by the compressibility of the gas phase. The plenum increases the gas volume of the system, which alternately accumulates by compression the mechanical energy of the system. In view of the results, it can be stated that the use of compressible gas and the inclusion of the plenum in the two-fluid model simulations clearly improves the results compared to those of the incompressible gas simulations. Figure 3b shows the normalized bed volume, for the compressible case with plenum, as a function of the vibration phase for three meshes with cells of 2, 4 and 8 mm side. It can be observed that the results remain practically unchanged when the cell size is reduced from 4 mm to 2 mm. However, the computational cost of the mesh with cells of 2 mm side is dramatically increased. Therefore, the simulation with compressible gas with plenum and a mesh with cells of 4 mm side will be taken as the base case in the subsequent analyses.

Concerning bubble behavior, Figure 4 shows four consecutive snapshots of a bubble rising in the experimental bed (Exp. 1) and a bubble of similar diameter rising in the simulation (Case-3). The location of the centroid of the bubble is also indicated on each of the images. As the bubble of the simulation raises in the bed, its position and diameter are influenced by vibration. The bubble rises faster in the first half of the period, comprising the first two images in each row of Figure 4 (from $\phi = 0$ to $\phi = \pi$), than in the rest of the cycle. Also, in the second half of the period (between $\phi = \pi$ and $\phi = 2\pi$) the shape of the bubble changes and its wake partially penetrates into the bubble. The same oscillatory behavior and wake penetration are found in the experimental snapshots of Figure 4b. The differences observed in terms of bubble shape may be attributed to the two-dimensionality of the model. In the experiments, the amount of particles raining in the bubble is increased by the presence of the front and rear walls. This raining phenomenon is difficult to capture in detail by the two fluid simulations due to the discrete nature of particle dynamics when the void

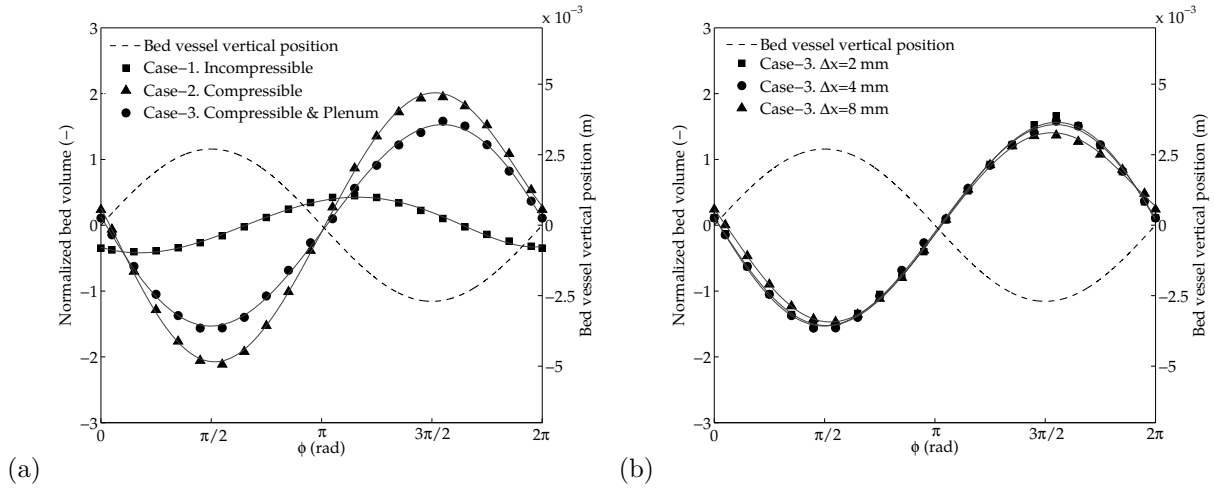

Figure 3: Normalized bed vessel position and bed volume as a function of the vibration phase. (a) Experimental results (Exp-1), incompressible gas phase model (Case-1), compressible gas phase model without plenum (Case-2) and compressible gas phase model with plenum (Case-3). (b) Case-3 for three different mesh resolutions. $f = 13.9$ Hz and $A = 2.7$ mm.

fraction is high. Sensitivity tests for the different mesh sizes, not shown here for simplicity, revealed that the bubble shape in the simulation is weakly affected when doubling the resolution of the mesh of Figure 4a.

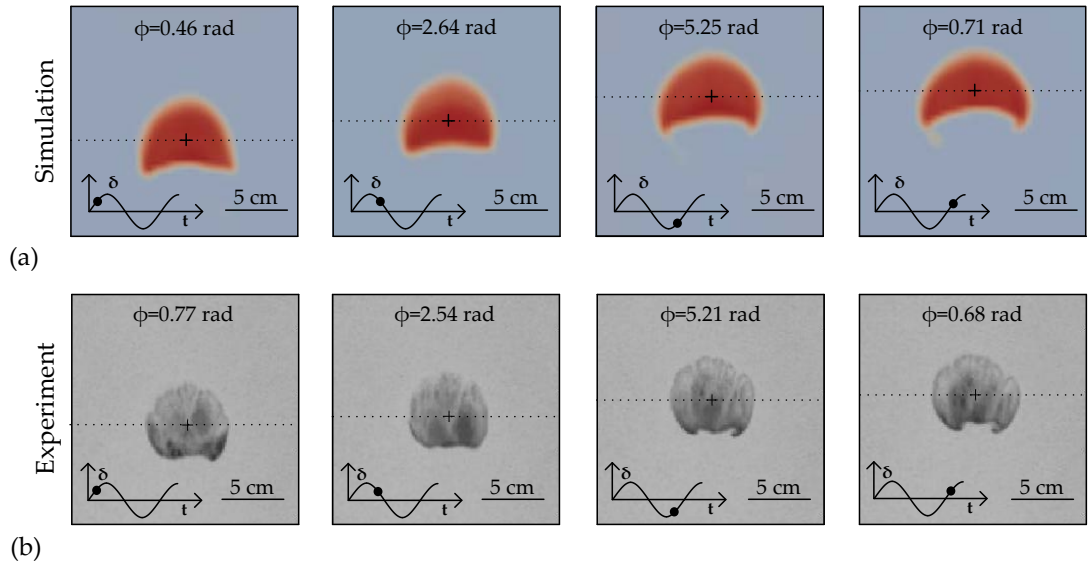

Figure 4: (a) Simulation snapshots (Case-3) and (b) grayscale digital images (Exp. 1) of an isolated bubble rising in the vibrating fluidized bed and captured at different vibration phases. The dotted horizontal line indicates the vertical position of the bubble centroid. The vertical displacement δ of the bed vessel is also indicated. $f = 13.9$ Hz, $A = 2.7$ mm.

5.2. Oscillatory bubble diameter

To analyze more quantitatively the bubble size oscillations, Figure 5 shows the averaging of cycles oscillations of the normalized bubble diameter for the simulated cases with incompressible gas, compressible gas without plenum and compressible gas with plenum (Cases 1-3). In order to make the results independent of the bubble size, normalization is carried out at each time instant in terms of the moving average of the bubble diameter $\overline{D}_b$, that is:

$$\Delta D_{bi} = \frac{D_{bi} - \overline{D}_{bi}}{\overline{D}_{bi}} \tag{9}$$

where i indicates the simulation frame or experimental image number.

It can be clearly observed in Figure 5a that the use of incompressible gas in the simulation fails to predict the phase of the oscillations of bubble diameter. In this case, the simulated bubble diameter tends to grow when the bed surface is moving upwards (see Figure 3), just the opposite to the experimental results. Also, contrary to the experimental observations, the incompressibility of the gas yields no phase delay between the lower half section of the bed ($z = 0.1 - 0.275$ m) and its higher half section ($z = 0.275 - 0.45$ m).

In contrast, the simulations with compressible gas, Figure 5b, are able to predict diameter oscillations with a phase closer to the experiments than the incompressible gas simulations. It can be appreciated in Figure 5b that there is a positive delay of the oscillation of bubble diameter when passing from the lower half of the bed to the upper half of the bed. This positive delay also happens in the experiments. Similarly to Figure 3, the presence of the plenum in the simulated domain promotes a softening in the oscillating movement of the whole bed, which is also reflected through a decrease in the amplitude of the bubble diameter fluctuations. Differences between the phases and amplitudes of the compressible gas simulations and the experiment could be attributed to the friction caused by the front and rear walls in the experiments [41–43], which can retard the phase of the oscillation and diminish their amplitude. This effect is not present in the two-dimensional simulation since it lacks of front and rear walls.

The effect of the bed vessel vibration amplitude and frequency on bubble diameter can be also studied through the averaging of cycles method. Figures 6 and 7 show the simulation and experimental results concerning the averaged oscillation of bubble diameter as a function of the amplitude (Figure 6) and the frequency (Figure 7) of the bed vessel vibration. The growth of the amplitude of the bubble diameter oscillations with the vibration amplitude observed in the experiments is well reproduced in the numerical model (see Figure 6a). Though the simulations predict amplitudes similar in the lower part of the bed to those of the experiments (Figure 6b), the amplitude of the oscillations in the upper part of the bed is always overpredicted by the simulated bed. This effect is also observed in Figure 7. According to the previous comments, the larger oscillation amplitude of the simulation could be explained with the lack of front and rear wall interaction in the simulated VFB. In the experiments, the friction of the bed material with the

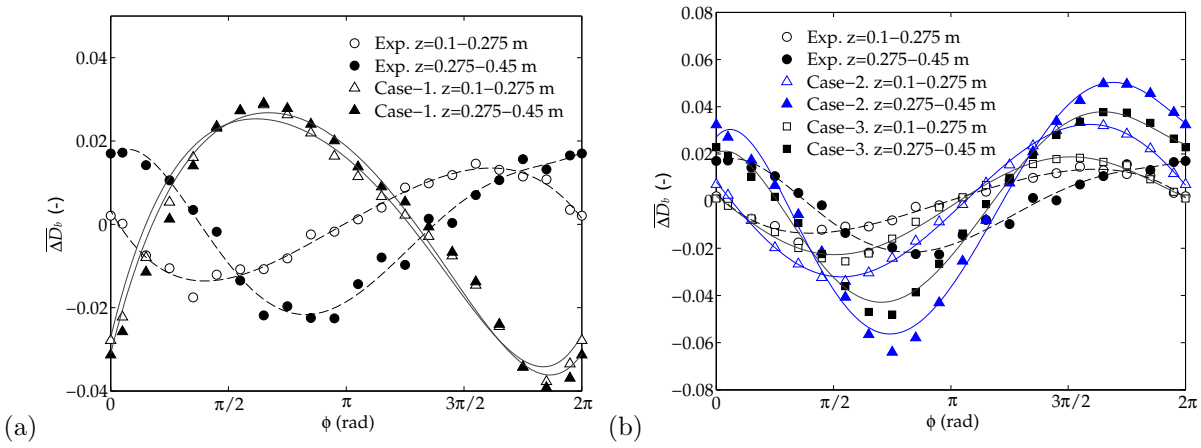

Figure 5: Normalized oscillation of bubble diameter as a function of the vibration phase. (a) Simulations with incompressible gas phase (Cases 1 and 2) (b) Simulations with compressible gas without and with plenum (Cases 2 and 3). Experimental results are also included. $f = 13.9$ Hz and $A = 2.7$ mm.

front and rear walls avoids the bubble to freely oscillate and reduces the oscillation of the bubble diameter. Nevertheless, both the experiments and the simulations agree in the fact that the variation of vibration amplitude has a more pronounced effect on the amplitude of diameter oscillation than the variation of vibration frequency (Figures 7a and 7b). Concerning the phase of the oscillations, the simulation reflects that the retardation in phase of the oscillation of the bubble diameter (Figure 7a) is more noticeable in the upper half section of the bed than in the lower half section. This is also in agreement with the experimental results (Figure 7b).

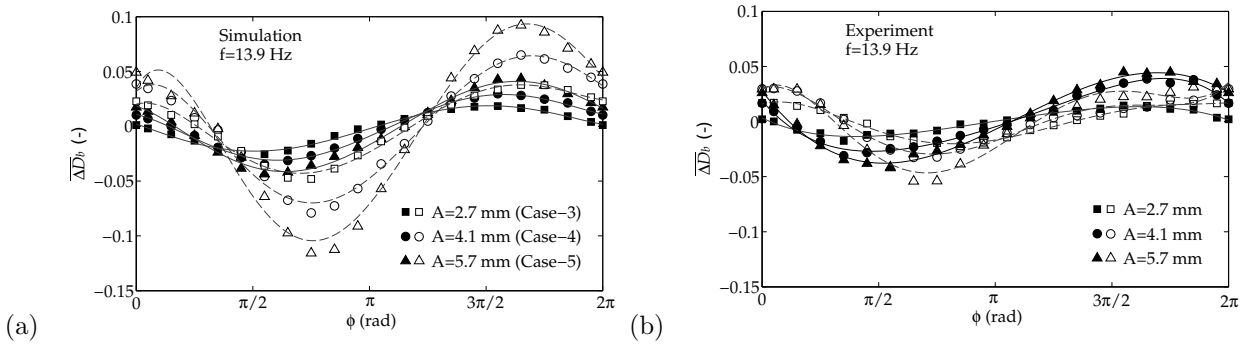

Figure 6: Normalized oscillation of bubble equivalent diameter as a function of the vibration phase for different vibration amplitudes (Cases 3, 4, and 5). (a) Simulation and (b) experimental results. The black symbols indicate the results for the lower half section of the bed ($z = 0.1 - 0.275$ m) and the white symbols for the upper half section ($z = 0.275 - 0.45$ m).

The value of the phase delay of bubble characteristics was calculated following the procedure indicated in Section 4.3. Note that in the simulations with incompressible gas-phase (Case-1) bubble characteristics do not present a phase delay between the lower and the higher half sections (Figure 5). This unrealistic result

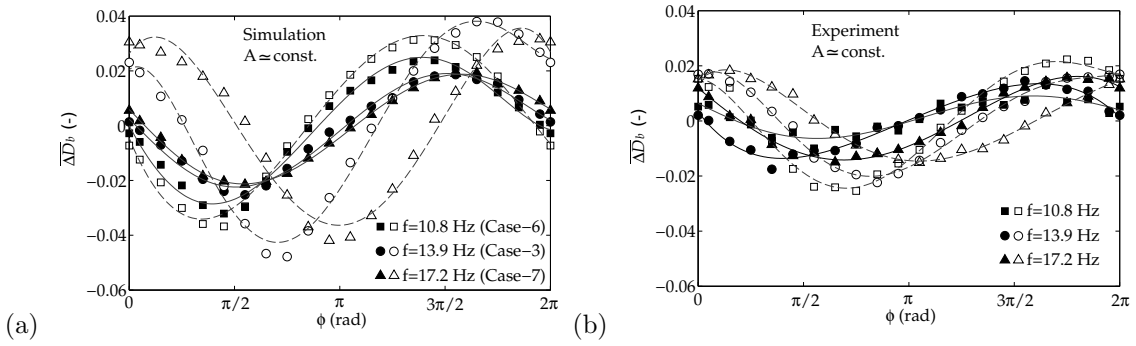

Figure 7: Normalized oscillation of bubble equivalent diameter as a function of the vibration phase for different vibration frequencies (Cases 3, 6, and 7). (a) Simulation and (b) experimental results. The black symbols indicate the results for the lower half section of the bed ($z = 0.1 - 0.275$ m) and the white symbols for the upper half section ($z = 0.275 - 0.45$ m).

is caused by the lack of compressible waves in the gas phase when the gas density is assumed constant.

Figure 8 shows the phase delay of the bubble diameter, in the upper and lower sections of the bed, as a function of the bed vessel vibration amplitude and frequency. It can be observed in the figure that the bubble oscillation delays of the simulation with the compressible gas model are in good agreement with the experimental observations. In particular, it can be seen in Figure 8 that the delay of the bubble oscillation with respect to the vessel displacement is about $\phi_d = \pi$ in both the simulation and the experiments. In view of Figure 3, where the bed volume also has a delay of π, it can be said that the compression-expansion of the bed bulk is the principal cause of the oscillation of the bubble diameter. Besides, for all the cases shown in Figure 8, bubble characteristics in the lower half of the bed present a lower phase delay than bubbles in the upper half, and this is finely reproduced by the compressible gas simulation. The delay of the diameter oscillations in the higher half of the bed is slightly smaller than the experimental results. This may be attributed to the absence of the front and rear walls in the two-dimensional numerical model, which retard the response of the dense phase with respect to the bed vessel oscillation movement. Another cause of the discrepancies concerning the delay of diameter oscillation could be the differences in the way the bubble contours are defined in the simulations and in the experiments. In the experiments the bubble contours are sharper than in the simulations due to the discrete nature of particles in a real bed.

Nevertheless, the retardation produced by the front and rear walls, or other causes, is not greatly contributing to the delay since it is acceptably well reproduced by the two-dimensional simulations, excepting perhaps at low frequencies (Case 6 in Figure 8b) where the energy introduced by vibration is smaller. All this facts confirmed by the numerical simulation support the assumption of the presence of compression-expansion waves traveling through the bed and propagating the information. As in [25], the propagation velocity of the simulated bubble diameter (i.e. the velocity of the compression wave in the bed bulk) can be calculated as the distance between the centres of the upper and lower sections of the bed times the vibration

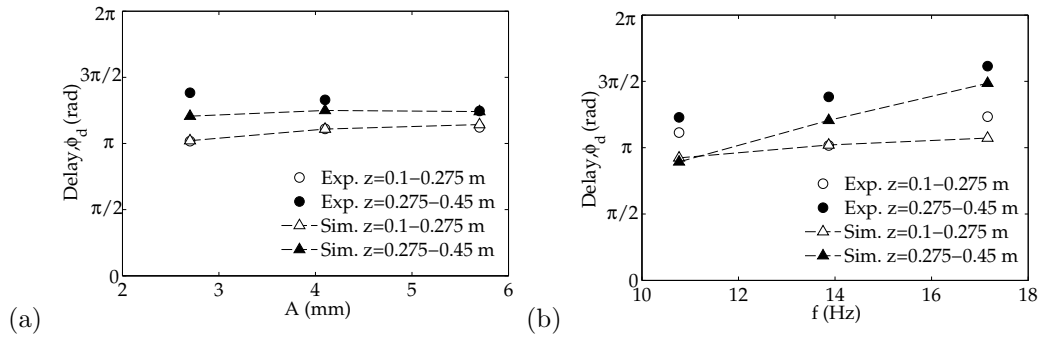

Figure 8: Phase delay of bubble equivalent diameter at different heights and comparison with experiments. (a)Variation with vibration amplitude (Cases 3, 4 and 5), (b) variation with vibration frequency (Cases 3, 6 and 7).

frequency and divided by the phase delay difference between those sections:

$$V_{prop} = 2\pi f \frac{\Delta z}{\Delta \phi} \tag{10}$$

Performing this operation for the simulation results in Figure 8, excluding the anomalous result at low frequency (Case 6), yields an average propagation velocity of $V_{prop,D_b,sim} = 31.2$ m/s for the simulation results and $V_{prop,D_b,exp} = 22.6$ m/s for the experiments. Despite the complexity of the simulated system and the absence of front and rear walls interactions in the 2D computations, these simulation and experimental results are reasonably similar and are of the same order of magnitude as the effective sound propagation velocity inside a fluidized bed, which can be calculated following [34] and is equal to 13.1 m/s.

5.3. Oscillatory bubble velocity

The bubble vertical rising velocity is studied using the same averaging of cycles methodology as in Section 5.2. Figure 9 shows the oscillation of the bubble vertical velocity normalized with the moving average of the bubble velocity ($\Delta V_{bi} = (V_{bi} - \overline{V}_{bi})/\overline{V}_{bi}$). The results for the simulation with incompressible gas (Figure 9a) and the compressible gas with and without plenum (Figure 9b) are compared with the experimental results. It can be seen how the simulation with the incompressible gas model fails to predict both the phase and the amplitude of the velocity oscillations. Additionally, no delay and amplitude variations are observed between the upper and lower half sections of the bed in the incompressible gas simulations, which corroborates the assumption that the change of the oscillation phase of bubble characteristics is mainly induced by the compression and expansion of the gas phase inside the bed.

According to Figure 9b, the two-fluid model simulations with compressible gas model clearly improve the prediction of the bubble velocity oscillation compared to the simulations with incompressible gas model. The simulations with compressible gas are able to reasonably match the experimental results in terms of phase

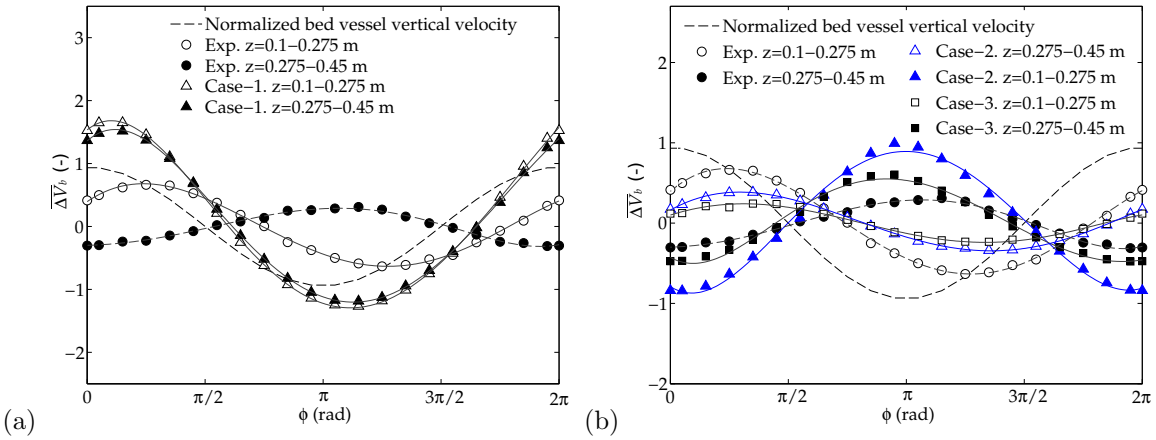

Figure 9: Normalized oscillation of bed vessel velocity and bubble absolute vertical velocity as a function of the vibration phase. (a) Simulations with incompressible gas phase (Cases 1 and 2) (b) Simulations with compressible gas without and with plenum (Cases 2 and 3). Experimental results are also included. $f = 13.9$ Hz and $A = 2.7$ mm.

delay and amplitude of the velocity oscillations. The simulations predict a higher amplitude of the velocity oscillation in the upper section of the bed, which could be attributed, as commented for the case of diameter oscillation, to the lack of front and rear walls in the simulation. The higher amplitude of velocity oscillations in the simulations might be also attributed to other effects such as the invariance of pressure imposed in the simulation at the top outlet of the bed, which is an approximation of what is actually occurring in a real VFB. However, the similarities between experiments and simulations are more than remarkable, given the complexity of the VFB system.

Similarly to the diameter fluctuation in Figure 5, the presence of the plenum in the computational domain 5 reduces the magnitude of the velocity oscillations in both sections of the bed in Figure 9. It can be seen in the figure that the introduction of the plenum in the simulation leads to results closer to the experiments.

The velocity fluctuations for the different vibration frequencies and amplitudes tested are also studied in Figures 10 and 11. The simulations with compressible gas and plenum yield a good estimation of the variation of the velocity fluctuation amplitude observed in the experiments when the amplitude of the vibration is increased. The amplitude of the normalized velocity increases in the upper and the lower sections of the bed for both the simulation (Figure 10a) and experimental results (Figure 10b). Also, in consonance with the experimental evidence, no great changes in the phase delay of the oscillations are observed when the vibration amplitude is varied. The effect of the vibration frequency in the normalized velocity oscillations observed in the experiments (Figure 11b) is also reasonably well reproduced in the simulations (Figure 11a). Quantitatively, the simulation predicts smaller oscillations in the lower half section of the bed and greater oscillations in the upper section of the bed.

Figure 12 shows the values of the phase delays of the bubble velocity fluctuations with respect to the

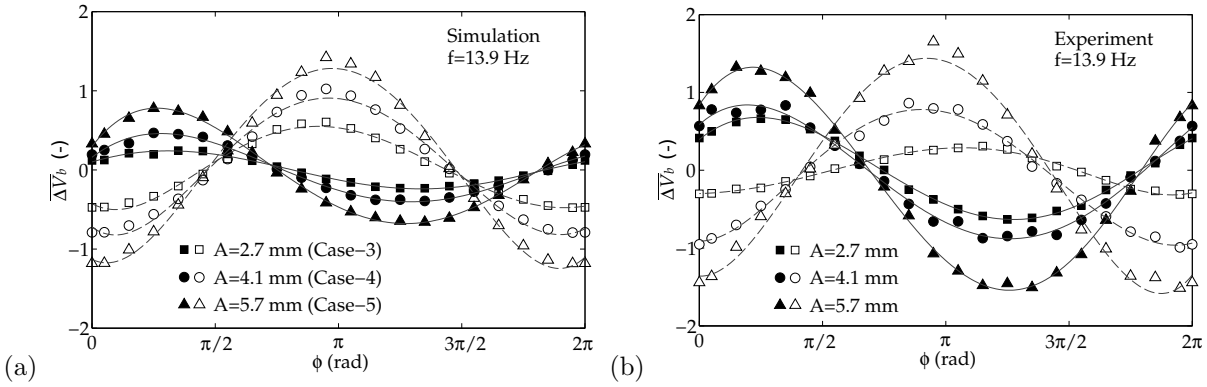

Figure 10: Normalized oscillation of bubble absolute vertical velocity as a function of the vibration phase for different vibration amplitudes (Cases 3, 4, and 5). (a) Simulation and (b) Experimental results. The black symbols indicate the results for the lower half section of the bed ($z = 0.1 - 0.275$ m) and the white symbols for the upper half section ($z = 0.275 - 0.45$ m).

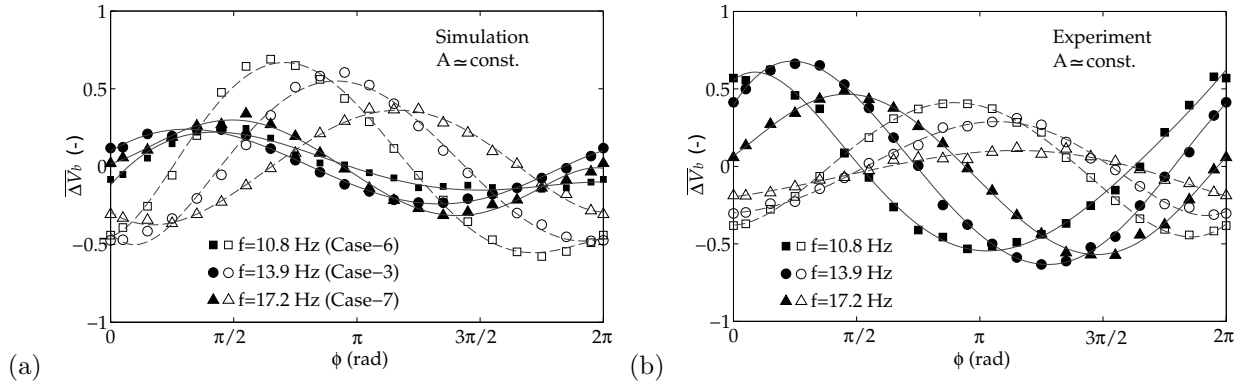

Figure 11: Normalized oscillation of bubble absolute vertical velocity as a function of the vibration phase for different vibration frequencies (Cases 3, 6, and 7). (a) Simulation and (b) Experimental results. The black symbols indicate the results for the lower half section of the bed ($z = 0.1 - 0.275$ m) and the white symbols for the upper half section ($z = 0.275 - 0.45$ m).

bed vessel velocity. Results are presented for both the lower and the upper half sections of the bed. The simulations yield an excellent estimation of the delay on bubble characteristics in most of the cases. As the small delay for $z = 0.1 - 0.275$ m in Figure 12a suggests, the bubble velocity close to the distributor seems to be more attached to the movement of the bed vessel than bubbles near the bed surface. While the simulation delays on Figure 12a are practically unaffected by the vibration amplitude, those in Figure 12b present a stronger variation with frequency. All these results are in harmony with experiments. The mean propagation velocity (Equation (10)) corresponding to the simulated bubble velocity fluctuations is $V_{prop,V_b,sim} = 10$ m/s. This is in good agreement with the same result calculated with the experimental data, $V_{prop,V_b,exp} = 6.9$ m/s. As for the case of diameter oscillations, these velocities are of the same order of magnitude as the effective sound propagation velocity in a fluidized bed.

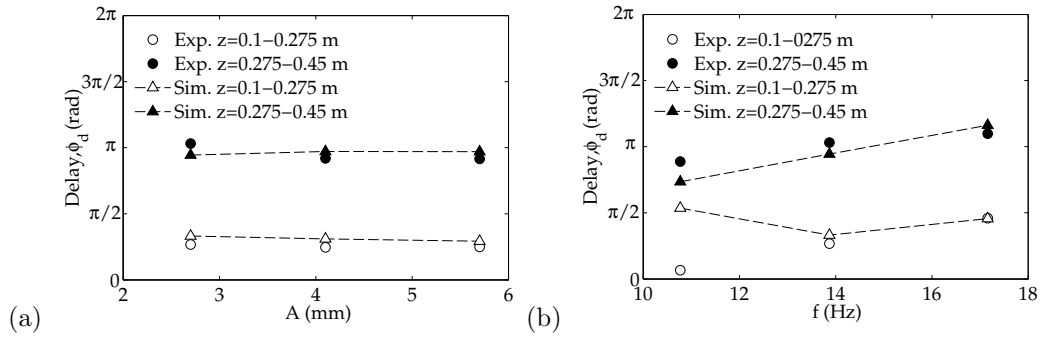

Figure 12: Phase delay of bubble absolute vertical velocity at different heights and comparison with experiments. (a)Variation with vibration amplitude (Cases 3, 4 and 5), (b) variation with vibration frequency (Cases 3, 6 and 7).

6. Conclusions

The size and motion of isolated bubbles rising in a pseudo-2D bed were numerically studied by means of two-fluid model simulations and compared with experiments. An averaging of cycles method was employed as a tool to analyze the local fluctuations of the bed bulk and bubble characteristics. Using this method, the simulations allowed to analyze the impact of the gas compressibility and the plenum in the bed and bubble behaviors. The results revealed that the simulation with incompressible gas is unable to reproduce the cyclic compression and expansion of the bed bulk and the delay of the isolated bubble diameter and velocity oscillations. In contrast, the two-fluid simulation resorting to the compressible gas model clearly reproduces the experimental results of the VFB system analyzed. The phase delays and amplitudes of the oscillations of the bubble diameter and velocity change with the bubble distance to the distributor. Thanks to the simulation evidence, these effects can be clearly attributed to the compressibility of the gas-phase. Besides, the simulations revealed that the presence of the plenum in the numerical model promotes a softening of the amplitude of the bed and bubble oscillations. As in the experiments, the numerical results indicate that the frequency at which the bed vessel is vibrated has a strong impact on the phase delay of the bubble diameter and velocity oscillations with respect to the bed vessel displacement, whereas the magnitude of these oscillations is mainly affected by the amplitude of the bed vessel oscillations. Most of the simulation results using the compressible gas model with plenum are quite similar to the experimental observations, which is remarkable given the complexity of the VFB system. However, some quantitative discrepancies between the simulations and the experiments were found, regarding the magnitude of the oscillations of bubble diameter and velocity. This may be attributed to the fact that the simulations were performed in two dimensions whereas the experimental pseudo-2D bed can be affected by the particles interaction with the front and rear walls of the bed vessel. Other effects such as the differences in the way the bubble contours are defined in the simulation and the experiments, might contribute to these discrepancies and their impact

on results should be studied in future works. The results here presented reveal the potential of the two-fluid model for the simulation of medium and large scale VFBs and suggest the need of incorporating the gas-phase compressibility to the simulation of bed and bubble oscillations in VFBs and other vibrating-like systems.

Nomenclature

$\boldsymbol{a}(t)$ = instantaneous acceleration (m/s^2)
A = vibration amplitude (mm)
A_{ap} = bed cross-sectional area, WK (m^2)
D_b = bubble equivalent diameter (m)
$\overline{D}_b$ = moving average of D_b (m)
d_p = particle diameter (μm)
e = restitution coefficient (-)
f = vibration frequency (Hz)
$\boldsymbol{f}_{eq}$ = equivalent mass force (m/s^2)
g = gravity acceleration constant (m/s^2)
g_0 = radial distribution function (-)
h_0 = settled bed height (m)
H = bed vessel height (m)
H_{eq} = equivalent plenum height (m)
$\boldsymbol{I}$ = unit tensor (-)
$\boldsymbol{I}_{gp}$ = inter-phase momentum exchange (kg/m^{2}s^2)
I_{2Dg} = second order deviatory tensor (s^{-2})
K = bed thickness (m)
N_{tot} = total number of phase intervals (-)
N_ϕ = number of cycles (-)
R_g = ideal gas constant (J/K Kg)
t = time (s)
T = oscillation period, $1/f$ (s)
T_g = gas temperature (K)
U = velocity (m/s)
U_{mf} = minimum fluidization velocity (m/s)
V_b = bubble velocity (m/s)
$\overline{V}_b$ = moving average of V_b (m/s)

V_{ap} = plenum chamber volume (m^3)

V_{prop} = propagation velocity of oscillations (m/s)

W = bed width (m)

$y(t)$ = instantaneous value of a variable

$\overline{y}(t)$ = moving average of y

z = vertical distance to the distributor (m)

z_b = bubble centroid vertical coordinate (m)

Greek letters

$\delta(t)$ = bed vessel vertical displacement (m)

Δt_{exp} = data export time-step (s)

Δy = oscillation of y

$\overline{\Delta y}$ = average oscillation of Δy

ε = volume fraction (-)

ε_0 = initial bed void fraction (-)

$\varepsilon_{p,th}$ = threshold of solid volume fraction (-)

ε^* = packed bed void fraction (-)

ϕ = phase (rad)

ϕ_d = phase delay (rad)

Φ = specularity coefficient (-)

θ = angle of internal friction (^{o})

Θ = granular temperature (m^2/s^2)

κ_Θ = granular temperature diffusion coefficient (kg/m s)

μ = viscosity (Pa s)

ρ = density (kg/m^3)

$\boldsymbol{\tau}$ = stress tensor (Pa)

ω = angular velocity (rad/s)

Subscripts

exp = experiment

g = gas phase

i = frame index

p = particle (solid) phase

sim = simulation

Acknowledgments

This work has been partially funded by the Spanish Government (Project DPI2009-10518) and the Autonomous Community of Madrid (Project S2009/ENE-1660).

References

[1] D. Kunii, O. Levenspiel, Fluidization Engineering: Butterworth-Heinemann: Newton, MA, 1991.

[2] S.A. Sadiq, M. Asif, Fluidization of nano-powders: Effect of flow pulsation, Powder Technol. 225 (2012) 86-92.

[3] R.E. Rosenweig, Fluidization: hydrodynamic stabilization with a magnetic field, Science. 204 (1979) 57-60.

[4] G.N. Jovanovic, Z.R. Jovanovic, Bubble size and fluidization regimes in magnetically controlled fluidized beds, paper no. 28i. AIChE Annual Meeting, St. Louis, MO, U.S.A. (1993).

[5] W. Nowak, M. Hasatani, M. Derczynski, Fluidization and heat transfer of fine particles in an acoustic field, AIChE Symp. Ser. 89 (1993) 137-149.

[6] R. Gupta, A.S. Mujumdar, Aerodynamics of a vibrated fluid bed, Can. J. Chem. Eng. 58 (1980) 332-338.

[7] S. Mori, A. Yamamoto, S. Iwata, T. Haruta, I. Yamada, E. Mizutani, Vibro-fluidization of group C particles and its industrial applications, AlChE Symp. Series. 86 (1990) 88-94.

[8] K. Noda, Y. Mawatari, S. Uchida, Flow patterns of fine particles in a vibrated fluidized bed under atmospheric or reduced pressure, Powder Technol. 99 (1998) 11-14.

[9] T. Zhou, H. Kage, S. Funaoka, H. Ogura, Y. Matsuno, Fluidization behaviour of glass beads under different vibration modules, Adv. Powder Technol. 12 (2001) 559-575.

[10] Y. Mawatari, Y. Tatemoto, K. Noda, Prediction of minimum fluidization velocity for vibrated fluidized bed, Powder Technol. 131 (2003) 66-70.

[11] N.J.M Kuipers, E.J. Stamhuis, A.A.C.M. Beenackers, Fluidization of potato starch in a stirred vibrated fluidized bed, Chem. Eng. Sci. 51 (1996) 2727-2732.

[12] Y. Mawatari, M. Tsunekawa, Y. Tatemoto, K. Noda, Favorable vibrated fluidization conditions for cohesive fine particles, Powder Technol. 154 (2005a) 54-60.

[13] A.S. Mujumbar, Handbook of Industrial Drying. Marcel Dekker. New York, 1987.

[14] C. Strumillo, Z. Pakowski, Drying of granular products in vibrofluidized beds, in: A.S. Mujumdar (Ed.), Drying'80: Developments in Drying, Hemisphere Publishing Corporation, Montreal, (1980) 211-226.

[15] C. Xu, J. Zhu, Experimental and theoretical study of the agglomeration arising from fluidization of cohesive particles-effects of mechanical vibration, Chem. Eng. Sci. 60 (2005) 6529-6541.

[16] X. Yang, Y. Zhao, Z. Luo, S. Song, C. Duan, L. Dong, Fine coal dry cleaning using a vibrated gas-fluidized bed, Fuel Process. Technol. 106 (2013) 338-343.

[17] Y. Mawatari, K. Tagawa, Y. Tatemoto, K. Noda, Bubbling characteristics under vertical vibration in a two-dimensional fluidized bed, Chem. Eng. Jpn. 38 (2005b) 18-23.

[18] T. Zhou, H. Kage, H. Li, Bubble characteristics in a two-dimensional vertically vibro-fluidized bed, China Particuology 3 (2005) 224-228.

[19] A. Acosta-Iborra, F. Hernández-Jiménez, M. de Vega, J.V. Briongos, A novel metodology for simulating vibrated fluidized beds using two-fluid models, Chem. Eng. J. 198-199 (2012) 261-274.

[20] E. Cano-Pleite, J. Gómez-Hernández, J. Sánchez-Prieto, A. Acosta-Iborra, Characterization of the Bubble Behavior in Vibrated Fluidized Beds by means of Two-Fluid CFD Simulations Coupled with Accelerometry Data, in The 14th International Conference on Fluidization - From Fundamentals to Products, Eds, ECI Symposium Series, Volume (2013).

[21] Y. Tatemoto, Y. Mawatari, T. Yasukawa, K. Noda, Numerical simulation of particle motion in vibrated fluidized bed, Chem. Eng. Sci. 59 (2004) 437-447.

[22] L. Xiang, W. Shuyan, L. Huilin, L. Goudong, C. Juhui, L. Yikun, Numerical simulation of particle motion in vibrated fluidized beds, Powder Technol. 197 (2010) 25-35.

[23] C. Zeilstra, M.A. van der Hoef, J.A.M. Kuipers, Experimental and numerical study of solids circulation in gas-vibro fluidized beds, Powder Technol. 248 (2013) 153-160.

[24] E.R.A. Eccles and A.S. Mujumdar, Bubble phenomena in aerated vibrated beds of small particles, Drying Technol. 15:1 (1997) 95-116.

[25] E. Cano-Pleite, F. Hernández-Jiménez, M. de Vega, A. Acosta-Iborra, Experimental study on the motion of isolated bubbles in a vertically vibrated fluidized bed, Chem. Eng. J. 255 (2014) 114-125.

[26] S. Limtrakul, W. Rotjanavijit, T. Vatanatham, Lagrangian modeling and simulation of effect of vibration on cohesive particle movement in a fluidized bed, Chem. Eng. Sci. 62 (2007) 232-245.

[27] Gidaspow D., Multiphase flow and Fluidization. Academic Press. Boston (1994).

[28] van Wachem B.G.M, Almstedt A.E., Methods for multiphase computational fluid dynamics, Chem. Eng. J. 96 (2003) 8198.

[29] M. Syamlal, W. Rogers, T.J. OBrien, MFIX Documentation: Theory Guide, U.S. Department of Energy (DOE), Morgantown Energy Technology Center, Morgantown, West Virginia, 1993.

[30] S. Benyahia, M. Syamlal, T.J. OBrien, Summary of MFIX Equations 2012-1, From URL https://mfix.netl.doe.gov/documentation/MFIXEquations2012-1.pdf, January 2012.

[31] D.G. Schaeffer, Instability in the evolution equations describing incompressible granular flow, J. Diff. Eqns. 66 (1987) 19-50.

[32] D. Musmarra, M. Poletto, S. Vaccaro, R. Clift, Dynamic waves in fluidized beds, Powder Technol. 82 (1995) 255-268.

[33] J. van der Schaaf, J.C. Schouten, C.M. van den Bleek, Origin, propagation and attenuation of pressure waves in gas-solid fluidized beds, Powder Technol. 95 (1998) 220-233.

[34] R. Roy, J.F. Davidson, V.G Tuponogov, The velocity of sound in fludised beds, Chem. Eng. Sci. 45 (1990) 3233-3245.

[35] S. Sasic, B. Leckner, F. Johnsson, Fluctuations and waves in fluidized bed systems: The influence of the air-supply system, Powder Technol. 153 (2005) 176-195.

[36] P.C. Johnson, R. Jackson, Frictional-collisional constitutive relations for granular materials, with application to plane shearing, J. Fluid Mech. 176 (1987) 67-93.

[37] I. Hulme, E. Clavell, L. van der Lee, A. Kantzas, CFD modeling and validation of bubble properties for a bubbling fluidized bed, Ind. Eng. Chem. Res. 44 (2005) 4254-4266.

[38] A. Boemer, H. Qi, U. Renz, Eulerian simulation of bubble formation at a jet in a two-dimensional fluidized bed, Int. J. Numer. Meth. Eng. 23 (1997) 927-944.

[39] F. Hernández-Jiménez, A. Gómez-García, D. Santana, A. Acosta-Iborra, Gas interchange between bubble and emulsion phases in a 2D fluidized bed as revealed by two-fluid model simulations, Chem. Eng. J. 215-216 (2013) 479-490.

[40] A. Busciglio, G. Vella, G. Micale, L. Rizzuti, Analysis of the bubbling behaviour of 2D gas solid fluidized beds: Part I. Digital image analysis technique, Chem. Eng. J. 140 (2008) 398-413.

[41] T. Li, J.R. Grace, X. Bi, Study of wall boundary condition in numerical simulations of bubbling fluidized beds, Powder Technol. 203 (2010) 447-457.

[42] F. Hernández-Jiménez, S. Sánchez-Delgado, A. Gómez-García, A. Acosta-Iborra, Comparison between two-fluid model

simulations and particle image analysis & velocimetry (PIV) results for a two-dimensional gas-solid fluidized bed, Chem. Eng. Sci. 66 (2011) 3753-3772.

[43] F. Hernández-Jiménez, J. Sánchez-Prieto, A. Soria-Verdugo, A. Acosta-Iborra, Experimental quantification of the particle-wall frictional forces in pseudo-2D gas fluidised beds, Chem. Eng. Sci. 102 (2013) 257-267.